

Pairing symmetry of an intermediate valence superconductor CeIr_3 investigated using μSR measurements

D. T. Adroja,^{1,2,*} A. Bhattacharyya,^{3,†} Y. J. Sato,^{4,5} M. R. Lees,⁶ P. K. Biswas,¹ K. Panda,³ Gavin B. G. Stenning,¹ A. D. Hillier,¹ and D. Aoki⁵

¹*ISIS Facility, Rutherford Appleton Laboratory, Chilton, Didcot Oxon, OX11 0QX, United Kingdom*

²*Highly Correlated Matter Research Group, Physics Department,*

University of Johannesburg, PO Box 524, Auckland Park 2006, South Africa

³*Department of Physics, Ramakrishna Mission Vivekananda Educational and Research Institute, Belur Math, Howrah 711202, West Bengal, India*

⁴*Graduate School of Engineering, Tohoku University, Sendai 980-8577, Japan*

⁵*Institute for Materials Research, Tohoku University, Oarai, Ibaraki 311-1313, Japan*

⁶*Department of Physics, University of Warwick, Coventry CV4 7AL, United Kingdom*

(Dated: February 18, 2022)

We have investigated the bulk and microscopic properties of the rhombohedral intermediate valence superconductor CeIr_3 by employing magnetization, heat capacity, and muon spin rotation and relaxation (μSR) measurements. The magnetic susceptibility indicates bulk superconductivity below $T_C = 3.1$ K. Heat capacity data also reveal a bulk superconducting transition at $T_C = 3.1$ K with a second weak anomaly near 1.6 K. At T_C , the jump in heat capacity $\Delta C/\gamma T_C \sim 1.39(1)$, is slightly less than the BCS weak coupling limit of 1.43. Transverse-field μSR measurements suggest a fully gapped, isotropic, s -wave superconductivity with $2\Delta(0)/k_B T_C = 3.76(3)$, very close to 3.56, the BCS gap value for weak-coupling superconductors. From the temperature variation of magnetic penetration depth, we have also determined the London penetration depth $\lambda_L(0) = 435(2)$ nm, the carriers' effective mass enhancement $m^* = 1.69(1)m_e$ and the superconducting carrier density $n_s = 2.5(1) \times 10^{26}$ carriers m^{-3} . The fact that LaIr_3 , with no $4f$ -electrons, and CeIr_3 with $4f^n$ electrons where $n \leq 1$ -electron (Ce ion in a valence fluctuating state), both exhibit the same s -wave gap symmetry indicates that the physics of these two compounds is governed by the Ir- d band near the Fermi-level, which is in agreement with previous band structure calculations.

PACS numbers: 71.20.Be, 75.10.Lp, 76.75.+i

I. INTRODUCTION

The strongly correlated electron systems of Ce, Yb, and U have attracted considerable attention in condensed matter physics, both theoretically and experimentally, due to the observation of heavy fermion (HF) and valence fluctuation behavior, unconventional superconductivity, quantum criticality, and spin and charge gap formation¹. The great interest in heavy fermion systems originated with the identification of superconductivity in CeCu_2Si_2 with $T_C = 0.7$ K in 1979 by Steglich *et al.*². At that time it was thought that magnetism and superconductivity would not occur simultaneously. Nevertheless, in CeCu_2Si_2 , the $4f$ electrons which give rise to the local magnetic moments also seem to be responsible for the unconventional superconductivity³. Unconventional superconductivity was also reported in other Ce-based heavy fermion compounds including CeCoIn_5 , which has a T_C of 2.3 K⁴, and the noncentrosymmetric HF superconductor CePt_3Si ⁵, a system without a center of inversion in the crystal structure that exhibits a coexistence of antiferromagnetic order ($T_N = 2.2$ K) and superconductivity ($T_C = 0.75$ K). Usually, the conventional BCS theory of superconductivity does not apply to these exotic systems⁶. Heavy fermions have a diverse range of ground states including superconductors such as UBe_{13} ⁷ and UPt_3 ^{8,9} which both adopt un-

conventional superconducting ground states. There are many magnetic HF systems which exhibit unconventional superconductivity under applied pressure. For example, CeIn_3 ($T_C = 1.2$ K at 2.46 GPa)¹⁰, CePd_2Si_2 ($T_C = 0.43$ K, at 30 GPa)¹¹, CeRh_2Si_2 ($T_C = 0.35$ K at 0.9 GPa)¹² and CeTX_3 ($T = \text{Co, Rh, Ir, X} = \text{Si and Ge}$; $T_C = 0.7 - 1.3$ K, 1-22 GPa)¹³⁻²². All these HF superconductors have very high upper critical fields and some of them exhibit anisotropic behavior. Furthermore, it is reported that the superconductivity in CeIn_3 (under pressure $T_C = 0.2$ K at 2.5 GPa) and CeCoIn_5 has d -wave pairing symmetry, mainly induced by the antiferromagnetic spin fluctuations, in a way that is very similar to the high-temperature cuprates. Strong interest in heavy fermions is also generated by the similarities seen in the phase diagrams of HF superconductors and high-temperature superconductors, including the cuprates and Fe-based materials²⁵⁻²⁸, where spin fluctuations are also suggested to play an important role.

Recently, $R\text{Ir}_3$ ($R = \text{La and Ce}$) based materials have attracted considerable attention both experimentally and theoretically due to the observation of superconductivity with strong spin-orbit coupling²⁹⁻³¹. CeIr_3 forms in a PuNi_3 -type rhombohedral crystal structure (Fig.1), space group $R\bar{3}m$ (166, D_{3d}^5)³⁰. Sato *et al.*³⁰ reported bulk type-II superconductivity in HF CeIr_3 , with a $T_C = 3.4$ K which is the second highest T_C among the Ce-

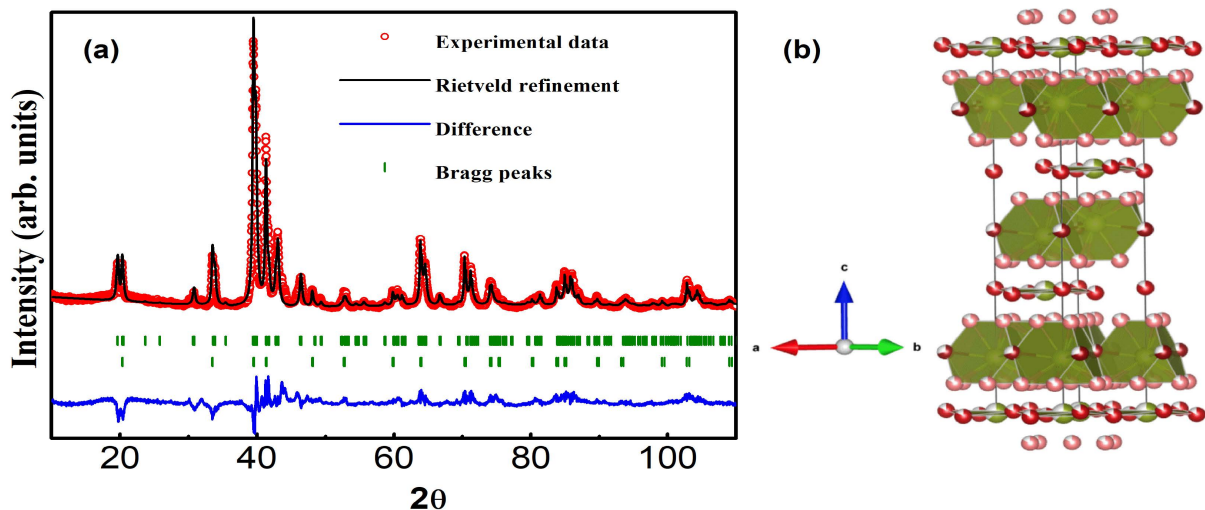


FIG. 1. (Color online)(a) Rietveld refinement of the X-ray diffraction pattern of CeIr_3 . The data are shown as red circles, and the result of the refinement as a solid line (black). We have used rhombohedral phase (space group $R\bar{3}m$, No. 166) of CeIr_3 as a main phase and added CeIr_2 cubic phase (space group $Fd\bar{3}m$, No. 227) as an impurity phase. The vertical green bars show the Bragg peaks' positions, top for CeIr_3 phase and bottom for CeIr_2 phase. (b) Rhombohedral crystal structure of CeIr_3 where the Ce atoms are the bigger spheres, and the Ir atoms are the smaller spheres.

based HF compounds. The crystal structure consists of two non-equivalent Ce sites (Ce1 and Ce2) and three Ir sites (Ir1, Ir2, and Ir3) (Fig.1b). Gornicka *et al.*³² calculated the band structure of CeIr_3 which confirmed a non-magnetic ground state, with a small contribution from the Ce 4*f* shell. It was reported that the density of states (DOS) at the Fermi surface principally arises from the 5*d* states of the Ir atoms, suggesting that CeIr_3 is indeed an Ir 5*d*-band superconductor and that the 5*d* electrons play a crucial role in the superconductivity.

The isostructural compound LaIr_3 , with $T_C = 2.5$ K, is another of the few materials^{29–31} with 5*d*-electrons that exhibits superconductivity. Here as well, the bands at the Fermi surface are dominated by the Ir 5*d* states with spin-orbit coupling, without any contribution from the La-orbitals; a similar situation is observed for CeRu_2 ³³. Very recently, we have investigated the superconducting properties of LaIr_3 using transverse-field (TF) and zero-field (ZF) muon spin rotation and relaxation (μSR) measurements. Our TF- μSR measurements revealed a fully gapped isotropic *s*-wave superconductivity with a gap to T_C ratio, $2\Delta(0)/k_B T_C = 3.31$, which is smaller than the value expected from the BCS theory of 3.56, implying weak-coupling superconductivity³¹. Moreover, zero-field- μSR measurements show there are no spontaneous magnetic field below T_C , which confirms time-reversal symmetry is preserved in LaIr_3 ³¹.

Here we have investigated the superconducting states of the mixed valence metal CeIr_3 by means of magnetization, heat capacity, and TF/ZF- μSR measurements. The temperature dependence of the magnetic penetration depth, determined by TF- μSR measurements, implies a fully gapped isotropic *s*-wave nature for the su-

perconducting state. The ZF- μSR data show no evidence of any spontaneous internal fields developing at and below T_C in the superconducting state, suggesting that time-reversal symmetry is preserved in the superconducting state of CeIr_3 .

II. EXPERIMENTAL DETAILS

A polycrystalline sample of CeIr_3 was prepared in a tetra arc furnace by arc melting stoichiometric quantities of the starting elements (Ce: 99.9 wt%; Ir: 99.999 wt%). The ingot was flipped and remelted five times, and the sample was quenched. The sample was subsequently annealed at 900^o for 6 days under a vacuum of 1×10^{-4} Pa in a quartz ampoule. The sample was wrapped in tantalum (Ta) foil during the annealing. The sample was heated to 900^oC and held at this temperature for 6 days and then quenched by switching off the furnace. The quality of the sample was verified through powder X-ray diffraction using a Panalytical X-Pert Pro diffractometer. The temperature and field dependence of magnetization was measured using a Quantum Design Magnetic Property Measurement System SQUID magnetometer; heat capacity down to 500 mK was measured using a Quantum Design Physical Property Measurement System with a ³He insert. To examine the superconducting pairing symmetry and microscopic superconducting properties of CeIr_3 , we performed TF/ZF μSR experiments at the muon beam line of the ISIS Pulsed Neutron and Muon Facility at the Rutherford Appleton Laboratory, United Kingdom using the MUSR spectrometer³⁴. The powder sample of CeIr_3 was mounted on a silver plate (99.995%)

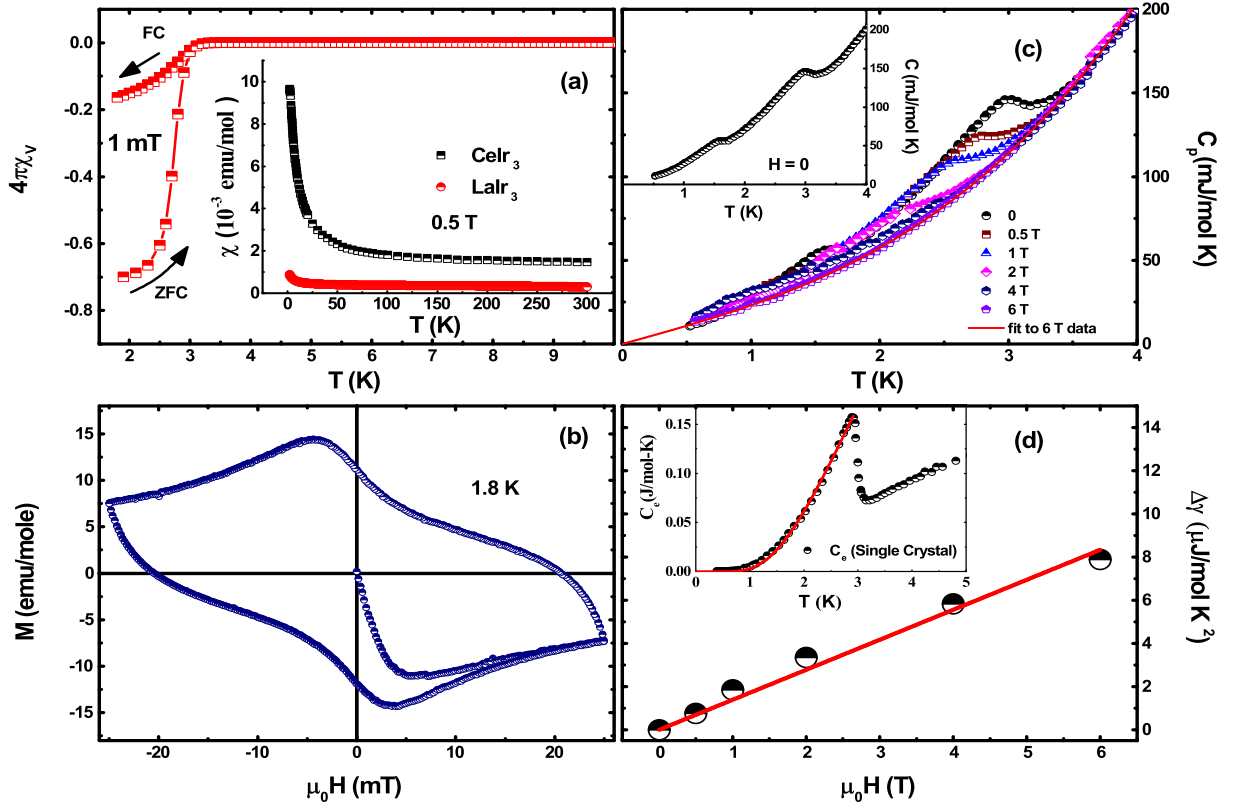


FIG. 2. (Color online)(a) DC magnetic susceptibility of CeIr_3 as a function of temperature in zero-field cooled (ZFC) and field-cooled cooling (FCC) mode. The inset shows the high-field magnetic susceptibility of CeIr_3 (black squares) and LaIr_3 (red circles). (b) Isothermal magnetic field dependence of the magnetization of CeIr_3 at 1.8 K. (c) Temperature dependence of the heat capacity of CeIr_3 at different applied fields. The solid line shows a fit to the 6 T data. The inset shows the temperature variation of the heat capacity in zero applied magnetic field. (d) Magnetic field dependence of the electronic specific heat $\Delta\gamma = [\gamma(H) - \gamma(0)]$ of CeIr_3 polycrystal sample extrapolated to $T \sim 0$ K. The solid line shows a linear behaviour indicating isotropic s-wave gap symmetry. Inset of (d) shows the electronic heat capacity for CeIr_3 single crystal from Ref. ³⁰ presented here for the comparison with the polycrystal data. The solid red line represents fully gapped superconductivity.

using GE varnish diluted with ethanol and covered with a silver foil. The sample was cooled to 50 mK using a dilution refrigerator. 100% spin-polarized positive muons were implanted into the sample and the asymmetry of the resulting decay positrons was estimated using, $P_z(t) = [N_F(t) - cN_B(t)]/[N_F(t) + cN_B(t)]$, where $N_B(t)$ and $N_F(t)$ are the number of positrons counted in the backward and forward detectors respectively and c is a instrumental calibration constant determined in the normal state with a small (2 mT) transverse magnetic field. The TF- μ SR data were collected in the different temperatures between 0.05 and 4 K in the presence of a 40 mT ($> \mu_0 H_{c1}(0) = 5.1(2)$ mT) magnetic field. ZF data were collected between 0.05 and 4 K. To reduce the impact of the magnetic fields at the sample position, correction coils were used which assured the stray fields were always less than 1 μ T. All the μ SR data were analyzed using WiMDA, a muon data analysis program³⁶.

III. RESULTS AND DISCUSSION

A. Crystal Structure and Physical properties

Fig.5 (a) presents the X-ray diffraction (XRD) pattern (symbols) and the Rietveld refinement fit (solid line) of the studied CeIr_3 compound. CeIr_3 crystallizes in the PuNi_3 -type rhombohedral structure with the space group $R\bar{3}m$. Our analysis of the XRD data reveals an impurity phase of CeIr_2 with a cubic structure (space group $Fd\bar{3}m$, No. 227) (see Fig.1a). The schematic unit cell obtained from Rietveld analysis of XRD data of CeIr_3 is shown in the inset of fig.5(b). The lattice parameters of the synthesized CeIr_3 sample are $a = 5.2943(2)$ Å and $c = 26.2134(1)$ Å, $\alpha = \beta = 90$ deg and $\gamma = 120$ deg which are in agreement with a previous report ³⁰.

Fig. 6(a) presents the temperature dependence of the magnetic susceptibility $\chi(T)$ in zero-field-cooled (ZFC) state and field-cooled (FC) state which confirms the bulk type-II superconductivity at 3.1 K in CeIr_3 . The isothermal magnetic field dependence of magnetization at 0.4 K

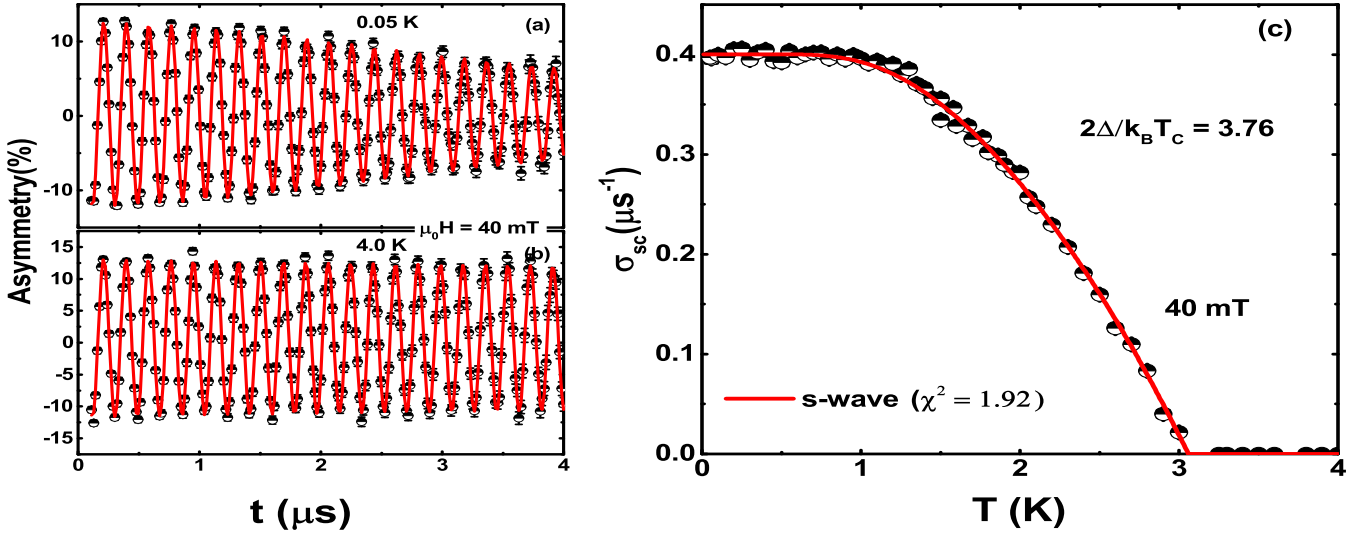


FIG. 3. (Color online) TF- μ SR spin precession signals for CeIr₃ collected in an applied transverse-magnetic field of $\mu_0 H = 40 \text{ mT}$. Asymmetry versus time in (a) the superconducting state at 0.05 K and (b) the normal state at 4.0 K. Solid lines represent fits to the data using Eq. 1. (c) Temperature variation of the Gaussian superconducting relaxation rate $\sigma_{sc}(T)$. The line is a fit to the data using an isotropic, fully gapped s -wave model using Eq. 2.

is shown in Fig. 6(b). Fig. 6(c) shows the temperature dependence of the heat capacity C_P at different applied magnetic fields. The inset in Fig. 6(c) shows the temperature variation of heat capacity at zero applied magnetic field. A clear signature of a superconducting transition is observed below 3.1 K in $C_P(T)$ data. Furthermore, another weak transition in $C_P(T)$ is seen below 1.6 K. As single crystal heat capacity of CeIr₃ shows only one transition at $T_C = 3.1 \text{ K}$ as shown in inset of Fig. 6(d), and no sign of second transition³⁰, which might suggest that the second transition observed in the polycrystalline CeIr₃ near 1.6 K might be related to a second superconducting impurity phase or very small variation on Ir composition (i.e. inhomogeneous Ir composition, CeIr_{3- δ})²⁹. Further, to check whether the transition near 1.6 K is coming from CeIr₂ phase or not, we have synthesised CeIr₂ polycrystalline sample and carried out XRD and heat capacity C_P (down to 400 mK) measurements. The results of XRD and C_P of CeIr₂ sample are given in the supplementary material (SM).³⁷ The C_P of CeIr₂ decreases with decreasing temperature from 2.5 K down to 400 mK and does not reveal any anomaly/peak due to an onset of superconductivity. This confirms that the weak anomaly observed in the heat capacity data of CeIr₃ near 1.6 K is not coming from the CeIr₂ phase and need further investigation. The jump in the heat capacity of CeIr₃ is suppressed in a magnetic field of 6 T. The heat capacity data were fitted using $C_P(T)/T = \gamma + \beta T^2$ where γ and β are electronic specific heat coefficient and lattice specific heat coefficient, respectively. The least squares fit yields $\gamma = 21.66(2) \text{ mJ}/(\text{mol}\cdot\text{K}^2)$, $\beta = 1.812(1) \text{ mJ}/(\text{mol}\cdot\text{K}^4)$, and then using $\beta = nN_A \frac{12}{5} \pi^4 R \Theta_D^{-3}$, where $R = 8.314 \text{ J}/\text{mol}\cdot\text{K}$ is the universal gas constant, n is the number of atoms per formula unit, and N_A is Avogadro's number, we estimate that the Debye temperature $\Theta_D = 162(2) \text{ K}$. Sato *et al.* have reported the heat capacity jump $\Delta C_P/\gamma T_C \sim 1.39(1)$ and $2\Delta(0)/k_B T_C = 3.83(1)$ ³⁰ for a single crystal of CeIr₃, which is closer to the theoretical BCS limit of a weak-coupling superconductor (3.56). Both of these values suggest that CeIr₃ can be categorized as a weak-coupling superconductor. Fig. 6(d) presents the magnetic field dependence of the electronic specific heat $\Delta\gamma [= \gamma(H) - \gamma(0)]$ extrapolated to $T \sim 0 \text{ K}$. The linear trend follows the behavior expected for a conventional BCS type superconductor. From the exponential dependence of C_e of CeIr₃ single crystal, as shown in the inset of Fig. 6(d), we obtained $2\Delta(0)/k_B T_C$ to be 3.81. The inset in Fig. 6(a) shows the high-field magnetic susceptibility measured up to 300 K for both CeIr₃ and LaIr₃. The susceptibility of CeIr₃ is higher than that of LaIr₃ and exhibits considerable temperature dependence below 25 K. The high temperature (50-300 K), weak temperature dependence, behavior of the susceptibility of CeIr₃ indicates the presence of strong hybridization between localized 4f-electron and conduction electrons and the mixed valence of the Ce ions. The low-temperature rise could be attributed to the Curie tail from an impurity. An X-ray photoelectron spectroscopy study reported that the Ce ions have a strongly intermediate valence character in CeIr₃³². The Ce ion valence of 3.6 in CeIr₃ was estimated using the superconducting transition temperatures, T_C , of the pseudo-binaries of the isostructural compounds LaIr₃, CeIr₃, and ThIr₃³³. Furthermore, evidence of an intermediate valence, between 3⁺ and 4⁺, of the Ce ions in CeIr₃ comes from Vegard's law by plotting the volume versus covalent radius of the R^{3+} metal in the $R\text{Ir}_3$ series. The volume increases monotonically with an increase in the radius, except for

gadolinium's number, we estimate that the Debye temperature $\Theta_D = 162(2) \text{ K}$. Sato *et al.* have reported the heat capacity jump $\Delta C_P/\gamma T_C \sim 1.39(1)$ and $2\Delta(0)/k_B T_C = 3.83(1)$ ³⁰ for a single crystal of CeIr₃, which is closer to the theoretical BCS limit of a weak-coupling superconductor (3.56). Both of these values suggest that CeIr₃ can be categorized as a weak-coupling superconductor. Fig. 6(d) presents the magnetic field dependence of the electronic specific heat $\Delta\gamma [= \gamma(H) - \gamma(0)]$ extrapolated to $T \sim 0 \text{ K}$. The linear trend follows the behavior expected for a conventional BCS type superconductor. From the exponential dependence of C_e of CeIr₃ single crystal, as shown in the inset of Fig. 6(d), we obtained $2\Delta(0)/k_B T_C$ to be 3.81. The inset in Fig. 6(a) shows the high-field magnetic susceptibility measured up to 300 K for both CeIr₃ and LaIr₃. The susceptibility of CeIr₃ is higher than that of LaIr₃ and exhibits considerable temperature dependence below 25 K. The high temperature (50-300 K), weak temperature dependence, behavior of the susceptibility of CeIr₃ indicates the presence of strong hybridization between localized 4f-electron and conduction electrons and the mixed valence of the Ce ions. The low-temperature rise could be attributed to the Curie tail from an impurity. An X-ray photoelectron spectroscopy study reported that the Ce ions have a strongly intermediate valence character in CeIr₃³². The Ce ion valence of 3.6 in CeIr₃ was estimated using the superconducting transition temperatures, T_C , of the pseudo-binaries of the isostructural compounds LaIr₃, CeIr₃, and ThIr₃³³. Furthermore, evidence of an intermediate valence, between 3⁺ and 4⁺, of the Ce ions in CeIr₃ comes from Vegard's law by plotting the volume versus covalent radius of the R^{3+} metal in the $R\text{Ir}_3$ series. The volume increases monotonically with an increase in the radius, except for

Ce, for which the unit cell volume is much smaller and comparable with the unit cell volume of GdIr_3 supporting the intermediate valence of Ce ion in CeIr_3 ³².

B. Superconducting gap structures

The TF- μSR asymmetry spectra measured in an applied magnetic field of 40 mT are displayed in Figs. 3(a-b). The data in Fig. 3(a) were taken at the base temperature in the superconducting state and in Fig. 3(b) at a higher temperature, well into the normal state. At $T \geq T_C$, the muon asymmetry oscillates with a very small damping, suggesting that the internal field distribution is extremely uniform. On the other hand, the asymmetry spectrum measured at $T \leq T_C$ shows an increased in damping, suggesting an inhomogeneous field distribution due to the vortex state. To obtain quantitative information about the superconducting state in CeIr_3 , we first tried to analyze TF- μSR data recorded at various temperatures using two Gaussian components, one to account CeIr_3 phase and another to account the impurity phase. However, two components model gave unphysical values of the parameters and fit did not converge. We therefore fitted our TF- μSR data using a single Gaussian model³⁸⁻⁴¹ given by,

$$G_x(t) = C_1 \cos(\omega_1 t + \Phi) \exp\left(\frac{-\sigma^2 t^2}{2}\right) + C_2 \cos(\omega_2 t + \Phi), \quad (1)$$

where C_i and ω_i ($i = 1, 2$), are the transverse-field asymmetries and the muon spin precession frequencies that arise from the sample and the silver sample holder (this could also include the impurity phase), and Φ and σ are a phase factor and total Gaussian depolarization rate, respectively. During the fitting C_2 was fixed at 35%, its low-temperature value, and the asymmetry spectra were then fit by varying the value of C_1 which is nearly independent of temperature. The phase, Φ , was also fixed to the value obtained at low temperature. Figs. 3(a-b) also include fits to the data (the solid red lines) using Eq. 1, show a good correspondence between the experimental and the calculated asymmetry spectra.

The values of σ determined from the fits consists of two parts; one part comes from the superconducting signal, σ_{sc} , and the other part is the nuclear magnetic dipolar contribution, σ_{nm} , which is taken to be constant over the entire temperature range studied. The superconducting depolarization rate σ_{sc} is then calculated using $\sigma_{sc} = \sqrt{\sigma^2 - \sigma_{nm}^2}$. The temperature variation of σ_{sc} shown in Eq. 1 is modeled using a standard expression within the local London approximation^{38,40,42} with

$$\begin{aligned} \frac{\sigma_{sc}(T)}{\sigma_{sc}(0)} &= \frac{\lambda^{-2}(T, \Delta_0)}{\lambda^{-2}(0, \Delta_0)} \\ &= 1 + \frac{1}{\pi} \int_0^{2\pi} \int_{\Delta(T)}^{\infty} \left(\frac{\delta f}{\delta E} \right) \times \frac{E dE d\phi}{\sqrt{E^2 - \Delta^2(T, \Delta)}} \end{aligned}$$

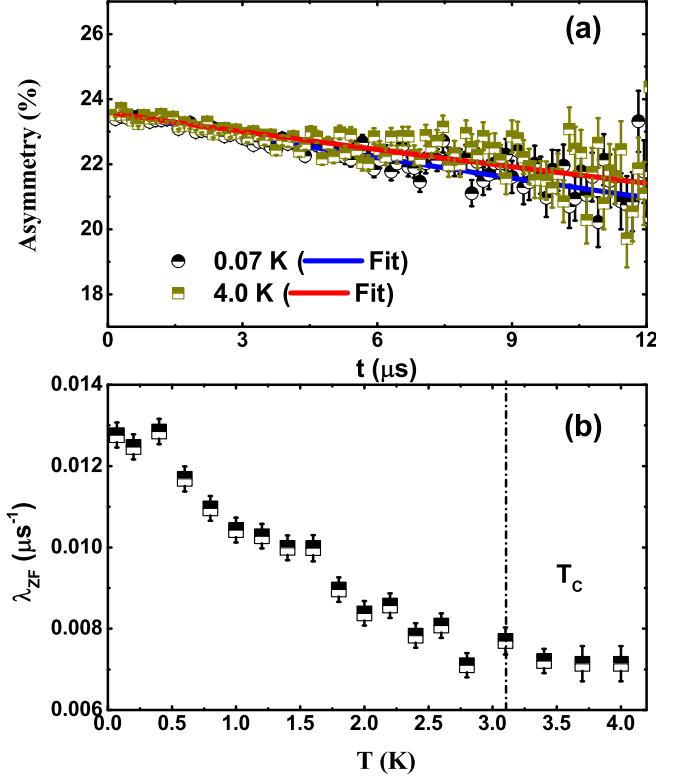


FIG. 4. (Color online) (a) Zero-field μSR asymmetry spectra for CeIr_3 collected at 0.07 K (black circles) and 4.0 K (dark yellow squares) together with lines that are least-squares fits the data using Eq. 3(b) Temperature variation of zero-field muon relaxation rate.

where $f = [1 + \exp(-E/k_B T)]^{-1}$ is the Fermi function, ϕ is the azimuthal angle in the direction of Fermi surface, and $\Delta(T, 0) = \Delta_0 \delta(T/T_C) g(\phi)$. Δ_0 , the gap value at zero temperature, is the only adjustable parameter. The temperature dependence of the gap can be approximated by $\delta(T/T_C) = \tanh[1.82[1.018(T_C/T - 1)]^{0.51}]$, and $g(\phi)$ gives the angular dependence of the gap function where ϕ is the polar angle for the anisotropy. The spatial dependence $g(\phi)$ is substituted by (a) 1 for an s -wave gap, and (b) $|\cos(2\phi)|$ for a d -wave gap with line nodes^{43,44}.

A conventional isotropically gapped model describes the data very well, as shown by the solid red line in Fig.3(c). Using this isotropic model, the refined critical temperature is $T_C = 3.1$ K and the gap to T_C ratio of $2\Delta(0)/k_B T_C = 3.76(3)$, is close to the value of 3.56 expected from a weak-coupling BCS theory. This value is in agreement with the heat capacity data.

Using the TF- μSR results, the other superconducting parameters characterizing the superconducting ground state of CeIr_3 can be evaluated. For a triangular lattice $\sigma_{sc}^2 = \frac{0.00371 \times \phi_0^2}{\lambda^4}$ where ϕ_0 is the flux quantum number $2.07 \times 10^{-15} \text{ T m}^2$ and γ_μ is the muon gyromagnetic ratio, $\gamma_\mu/2\pi = 135.5 \text{ MHz T}^{-1}$. Using this relation we have estimated the magnetic penetration depth,

TABLE I. Superconducting parameters of CeIr₃ and LaIr₃. The parameters values of LaIr₃ comes from Ref.³¹

Parameter	CeIr ₃	LaIr ₃
T_C (K)	3.1	2.5
$\mu_0 H_{c1}$ (mT)	5.1(2)	11.0(2)
$\mu_0 H_{c2}$ (T)	4.65(3)	3.84(2)
$\gamma(0)$ (mJ/mol K ²)	21.66(2)	15.32(3)
Θ_D	162(2)	430(4)
$\Delta C/\gamma T_C$	1.39(1)	1.0(2)
$2\Delta/k_B T_C$	3.76(3)	3.31(1)
λ (nm)	435(2)	386(3)
λ_{e-ph}	0.57(2)	0.53(3)
n_s (carriers/m ³)	$2.5(1) \times 10^{26}$	$2.9(1) \times 10^{27}$

$\lambda(0) = 435(2)$ nm. The London theory³⁵ gives the relation between microscopic quantities, λ (or λ_L), effective mass (m^*) and the superconducting carrier density (n_s); $\lambda_L^2 = \lambda^2 = \frac{m^* c^2}{4\pi n_s e^2}$, here $m^* = (1 + \lambda_{e-ph}) m_e$, where λ_{e-ph} is the electron-phonon coupling constant and m_e is an electron mass. Using McMillan's relation⁴⁵, λ_{e-ph} can be determined using

$$\lambda_{e-ph} = \frac{1.04 + \mu^* \ln(\Theta_D/1.45T_C)}{(1 - 0.62\mu^*) \ln(\Theta_D/1.45T_C) - 1.04}, \quad (2)$$

where Θ_D is the Debye temperature. Assuming a repulsive screened Coulomb parameter $\mu^* = 0.13$ ⁴⁶, we have estimated $\lambda_{e-ph} = 0.57(2)$. This value of λ_{e-ph} is larger than 0.02 to 0.2 observed for many Fe-based superconductors (11- and 122-family) and cuprates (YBCO-123)⁴⁷, but smaller than 1.38 for LiFeAs⁴⁸, 1.53 for PrFeAsO_{0.60}F_{0.12}⁴⁹ and 1.2 for LaO_{0.9}F_{0.1}FeAs⁵⁰. Given CeIr₃ is a type II superconductor, and using the above estimated value of λ_{e-ph} and λ_L , we have estimated the effective-mass enhancement $m^* = 1.69(1)m_e$ and superconducting carrier density $n_s = 2.5(1) \times 10^{26}$ carriers m⁻³. The superconducting parameters of CeIr₃ and LaIr₃ are collected together in Table I.

C. Zero-field muon spin relaxation

ZF- μ SR muon asymmetry spectra above (dark yellow) and below (black) T_C , that are representative of the data collected are shown in Figs. 4(a-b). Both spectra exhibit a slow and almost indistinguishable exponential relaxation. Fits to the ZF- μ SR spectra at several temperatures between 0.07 and 4.0 K were made using the Lorentzian function⁵¹⁻⁵⁴,

$$G_z(t) = C_0 \exp(-\lambda_{ZF}t) + C_{bg}, \quad (3)$$

where C_0 , C_{bg} and λ_{ZF} are the total initial asymmetry from muons probing the sample, the asymmetry arising from muons landing in the silver sample holder, and the electronic relaxation rate, respectively. The parameters C_0 , and C_{bg} are found to be temperature independent. The zero-field- μ SR measurements reveal the relaxation rate between 0.07 and 4 K is slightly temperature dependent, suggesting the presence of weak spin-fluctuations. This effect is not seen in LaIr₃, which suggests that the spin fluctuations originate from the Ce moments that are in intermediate valence state. There is no clear change in λ_{ZF} as the samples cools though T_C indicating that time-reversal symmetry is likely preserved in CeIr₃.

IV. SUMMARY

In summary, we have examined the superconducting properties, including the superconducting ground state, of CeIr₃. Magnetic susceptibility measurements show CeIr₃ is a bulk type-II superconductor with $T_C = 3.1$ K. The heat capacity of polycrystalline CeIr₃ shows the superconducting transition near 3.1 K and a second weaker anomaly near 1.6 K. Given that the heat capacity of CeIr₃ single crystal exhibits only one transition near $T_C = 3.1$ K²⁹ and no peak observed in the heat capacity of CeIr₂ between 2.5 K and 400 mK³⁷, the second transition near 1.6 K could be associated with some variation in Ir content throughout the sample and need further investigation. The temperature dependence of the ZF- μ SR relaxation rate confirmed the preservation of time-reversal symmetry below T_C ; the very weak temperature dependence suggests the presence of weak spin fluctuations. Transverse-field μ SR measurements reveal the CeIr₃ exhibits an isotropic fully gapped s -wave type superconductivity with a gap to T_C ratio, $2\Delta(0)/k_B T_C = 3.76$, compared to the expected BCS value of 3.56 suggesting weak-coupling superconductivity. The s -wave pairing symmetry observed in both LaIr₃³¹, a material with no $4f$ -electrons and CeIr₃, with less than one $4f$ -electron, indicates that the superconductivity is controlled by the Ir- d bands near the Fermi level in both the compounds.

V. ACKNOWLEDGMENTS

A. B. would like to thank DST India, for an Inspire Faculty Research Grant (DST/INSPIRE/04/2015/000169). D. T. A. and A. D. H. would like to acknowledge the CMPC-STFC, grant number CMPC-09108. D. T. A. is grateful to the JSPS for an invitation fellowship. K. P. would like to acknowledge DST India, for an Inspire Fellowship (IF170620).

- * devashibhai.adroja@stfc.ac.uk
† amitava.bhattacharyya@rkmvu.ac.in
- ¹ P. Coleman, *Introduction to Many-Body Physics*, (Cambridge University Press, Cambridge, 2015).
 - ² F. Steglich, J. Aarts, C. D. Bredl, W. Lieke, D. Meschede, W. Franz, and H. Schäfer, *Phys. Rev. Lett.* **43**, 1892 (1979).
 - ³ M. Smidman, O. Stockert, J. Arndt, G. M. Pang, L. Jiao, H. Q. Yuan, H. A. Vieyra, S. Kitagawa, K. Ishida, K. Fujiwara, T. C. Kobayashi, E. Schuberth, M. Tippmann, L. Steinke, S. Lausberg, A. Steppke, M. Brando, H. Pfau, U. Stockert, P. Sun, S. Friedemann, S. Wirth, C. Krellner, S. Kirchner, E. M. Nica, R. Yu, Q. Si, and Frank Steglich, *Phil. Mag.* **98**, 2930-2963 (2018).
 - ⁴ C. Petrovic, P. G. Pagliuso, M. F. Hundley, R. Movshovich, J. L. Sarrao, J. D. Thompson, Z. Fisk, and P. Monthoux, *J. Phys.: Condens. Matter* **13**, L337 (2001).
 - ⁵ E. Bauer, G. Hilscher, H. Michor, Ch. Paul, E. W. Scheidt, A. Griбанov, Yu. Seropegin, H. Nol, M. Sgrist, and P. Rogl, *Phys. Rev. Lett.* **92**, 027003 (2018).
 - ⁶ J. Bardeen, L. N. Cooper, and J. R. Schrieffer, *Phys. Rev.* **106**, 162 (1957).
 - ⁷ M. W. McElfresh, J. H. Hall, R. R. Ryan, J. L. Smith, and Z. Fisk, *Acta Cryst.* **C46**, 1579-1580 (1990).
 - ⁸ A. de Visser, J. J. M. Franse, and A. Menovsky, *J. Mag. Mag. Mat.* **43**, 1 (1983).
 - ⁹ T. Trappmann and H. v. Löhneysen, and L. Taillefer, *Phys. Rev. B* **43**, 13714 (1991).
 - ¹⁰ G. Knebel, D. Braithwaite, P. C. Canfield, G. Lapertot, and J. Flouquet *Phys. Rev. B* **65**, 024425 (2001).
 - ¹¹ N. D. Mathur, F. M. Grosche, S. R. Julian, I. R. Walker, D. M. Freye, R. K. W. Haselwimmer, and G. G. Lonzarich, *Nature*, London **394**, 39 (1998).
 - ¹² R. Movshovich, T. Graf, D. Mandrus, J. D. Thompson, J. L. Smith, and Z. Fisk, *Phys. Rev. B* **53**, 8241 (1996); S. Araki, M. Nakashima, R. Settai, T. C. Kobayashi, and Y. Ōnuki, *J. Phys.: Condens. Matter* **14**, L377 (2002).
 - ¹³ Y. Muro, D. Eom, N. Takeda, and M. Ishikawa, *J. Phys. Soc. Jpn.* **67**, 3601 (1998).
 - ¹⁴ N. Kimura, K. Ito, K. Saitoh, Y. Umeda, H. Aoki, and T. Terashima, *Phys. Rev. Lett.* **95**, 247004 (2005).
 - ¹⁵ N. Kimura, Y. Muro, and H. Aoki, *J. Phys. Soc. Jpn.* **76**, 051010 (2007).
 - ¹⁶ I. Sugitani, Y. Okuda, H. Shishido, T. Yamada, A. Thamizhavel, E. Yamamoto, T. D. Matsuda, Y. Haga, T. Takeuchi, R. Settai, and Y. Ōnuki, *J. Phys. Soc. Jpn.* **75**, 043703 (2006).
 - ¹⁷ Y. Okuda, Y. Miyauchi, Y. Ida, Y. Takeda, C. Tonohiro, Y. Oduchi, T. Yamada, N. D. Dung, T. D. Matsuda, Y. Haga, T. Takeuchi, M. Hagiwara, K. Kindo, H. Harima, K. Sugiyama, R. Settai, and Y. Ōnuki, *J. Phys. Soc. Jpn.* **76**, 044708 (2007).
 - ¹⁸ R. Settai, I. Sugitani, Y. Okuda, A. Thamizhavel, M. Nakashima, Y. Ōnuki, and H. Harima, *J. Magn. Magn. Mater.* **310**, 844 (2007).
 - ¹⁹ G. Knebel, D. Aoki, G. Lapertot, B. Salce, J. Flouquet, T. Kawai, H. Muranaka, R. Settai, and Y. Ōnuki, *J. Phys. Soc. Jpn.* **78**, 074714 (2009).
 - ²⁰ A. Thamizhavel, T. Takeuchi, T. D. Matsuda, Y. Haga, K. Sugiyama, R. Settai, and Y. Ōnuki, *J. Phys. Soc. Jpn.* **74**, 1858 (2005).
 - ²¹ T. Kawai, H. Muranaka, M.-A. Measson, T. Shimoda, Y. Doi, T. Matsuda, Y. Haga, G. Knebel, G. Lapertot, D. Aoki, J. Flouquet, T. Takeuchi, R. Settai, and Y. Ōnuki, *J. Phys. Soc. Jpn.* **77**, 064716 (2008).
 - ²² F. Honda, I. Bonalde, K. Shimizu, S. Yoshiuchi, Y. Hirose, T. Nakamura, R. Settai, and Y. Ōnuki, *Phys. Rev. B* **81**, 140507 (2010).
 - ²³ A. de Visser, M. J. Graf, P. Estrela, A. Amato, C. Baines, D. Andreica, F.N. Gyga, and A. Schenck, *Phys. Rev. Lett.* **85**, 3005 (2000).
 - ²⁴ V. A. Sidorov, M. Nicklas, P. G. Pagliuso, J. L. Sarrao, Y. Bang, A. V. Balatsky, and J. D. Thompson, *Phys. Rev. Lett.* **89**, 157004 (2002).
 - ²⁵ A. Grauel, A. Böhm, H. Fischer, C. Geibel, R. Köhler, R. Modler, C. Schank, F. Steglich, G. Weber, T. Komatsubara, and N. Sato, *Phys. Rev. B* **46**, 5818(R) (1992).
 - ²⁶ Q. Si, and F. Steglich, *Science*, **329**, 1161 (2010).
 - ²⁷ J. Zhao, Q. Huang, C. L. Clarina, L. Shiliang, J. W. Lynn, C. Ying, M. A. Green, G. F. Chen, G. Li, Z. Li, J. L. Luo, N. L. Wang, and D. Pengcheng, *Nat. Mater.* **7**, 953 (2008).
 - ²⁸ J. Paglione and R. L. Greene, *Nat. Phys.* **6**, 645 (2010).
 - ²⁹ N. Haldolaarachchige, L. Schoop, M. A. Khan, W. Huang, H. Ji, K. Hettiarachchilage, and D. P. Young *J. Phys.: Condens. Matter* **29**, 475602 (2017).
 - ³⁰ Y. J. Sato, A. Nakamura, Y. Shimizu, A. Maurya, Y. Homma, D. Li, F. Honda, and D. Aoki *J. Phys. Soc. Jpn.* **87**, 053704 (2018).
 - ³¹ A. Bhattacharyya, D. T. Adroja, P. K. Biswas, Y. J. Sato, M. R. Lees, D. Aoki, and A. D. Hillier, *J. Phys.: Condens. Matter* **32**, 065602 (2020).
 - ³² K. Gornicka, E. M. Carnicom, S. Golab, M. Lapinski, B. Wiendlocha, W. Xie, D. Kaczorowski, R. J. Cava, and T. Klimczuk, *Supercond. Sci. Technol.* **32**, 025008 (2019).
 - ³³ M. Hakimi, and J. G. Huber, *Physica B+C* **135**, 434 (1985).
 - ³⁴ S. L. Lee, S. H. Kilcoyne, and R. Cywinski, *Muon Science: Muons in Physics, Chemistry, and Materials* (SUSSP and IOP, Bristol, UK, 1999).
 - ³⁵ J. E. Sonier, J. H. Brewer, and R. F. Kiefl, *Rev. Mod. Phys.* **72**, 769 (2000).
 - ³⁶ F. L. Pratt, *Physica B* **289-290**, 710 (2000).
 - ³⁷ Supplementary Materials, D. T. Adroja, A. Bhattacharyya, Y. J. Sato, M. R. Lee, P. K. Biswas, K. Panda, Gavin G.B. Stenning, D. Aoki and A.D. Hillier, XRD and Heat capacity measurements on CeIr₂ polycrystalline sample.
 - ³⁸ A. Bhattacharyya, D. T. Adroja, J. Quintanilla, A. D. Hillier, N. Kase, and A. M. Strydom, and J. Akimitsu, *Phys. Rev. B* **91**, 060503(R), (2015).
 - ³⁹ A. Bhattacharyya, D. T. Adroja, N. Kase, A. D. Hillier, J. Akimitsu, and A. M. Strydom, *Sci. Rep.* **5**, 12926 (2015).
 - ⁴⁰ D. T. Adroja, A. Bhattacharyya, M. Telling, Y. Feng, M. Smidman, B. Pan, J. Zhao, A. D. Hillier, F. L. Pratt, and A. M. Strydom, *Phys. Rev. B* **92**, 134505 (2015).
 - ⁴¹ A. Bhattacharyya, D. T. Adroja, M. Smidman, and V. K. Anand, *Sci. China-Phys. Mech. Astron.* **61**, 127402 (2018).
 - ⁴² A. Bhattacharyya, D. T. Adroja, K. Panda, Surabhi Saha, Tanmoy Das, A. J. S. Machado, T. W. Grant, Z. Fisk, A. D. Hillier, and P. Manfrinetti, *Phys. Rev. Lett.* **122**, 147001 (2019).
 - ⁴³ J. F. Annett, *Adv. Phys.* **39**, 83 (1990).

- ⁴⁴ G. M. Pang, M. Smidman, W. B. Jiang, J. K. Bao, Z. F. Weng, Y. F. Wang, L. Jiao, J. L. Zhang, G. H. Cao, and H. Q. Yuan, *Phys. Rev. B* **91**, 220502(R) (2015).
- ⁴⁵ W. L. McMillan, *Phys. Rev.* **167**, 331 (1968).
- ⁴⁶ Philip B. Allen, in *Handbook of Superconductivity*, edited by C. P. Poole, Jr. (Academic Press, New York, 1999) Chp-9 pp. 478-483 (1999).
- ⁴⁷ A.-M. Zhang and Q.-M. Zhang, *Chin. Phys. B* **22**, 08710 (2013).
- ⁴⁸ A. A. Kordyuk, V. B. Zabolotnyy, D. V. Evtushinsky, T. K. Kim, I. V. Morozov, M. L. Kulić, R. Follath, G. Behr, B. Buchner, and S. V. Borisenko, *Phys. Rev. B* **83**, 134513 (2011)
- ⁴⁹ D. Bhoi, P. Mandal, and P. Choudhury, *Supercond. Sci. Technol.* **21**, 125021 (2008).
- ⁵⁰ G. Mu, X.-Y. Zhu, L. Fang, L. Shan, C. Ren, and H.-H. Wen, *Chin. Phys. Lett.* **25**, 2221 (2008).
- ⁵¹ D. T. Adroja, A. Bhattacharyya, P. K. Biswas, M. Smidman, A. D. Hillier, H. Mao, H. Luo, G.-H. Cao, Z. Wang, and C. Wang, *Phys. Rev. B* **96**, 144502 (2017).
- ⁵² D. T. Adroja, A. Bhattacharyya, M. Telling, Yu, M. Smidman, B. Pan, J. Zhao, A. D. Hillier, F. L. Pratt, and A. M. Strydom, *Phys. Rev. B* **92**, 134505 (2015).
- ⁵³ D. T. Adroja, A. Bhattacharyya, M. Smidman, A. D. Hillier, Yu, B. Pan, J. Zhao, M. R. Lees, A. M. Strydom, and P. K. Biswas, *J. Phys. Soc. Jpn.* **86**, 03470 (2016).
- ⁵⁴ A. Bhattacharyya, D. T. Adroja, A. D. Hillier, R. Jha, V. P. S. Awana, and A. M. Strydom, *J. Phys.: Condens. Matter* **29**, 265602 (2017).

Supplementary Materials: Pairing symmetry of an intermediate valence superconductor CeIr₃ investigated using μ SR measurements

x-ray diffraction and Heat Capacity measurements of CeIr₂

A polycrystalline sample of CeIr₂ was prepared in a tetra arc furnace by arc melting stoichiometric quantities of the starting elements (Ce: 99.9 wt%; Ir: 99.999 wt%). The ingot was flipped and remelted five times to improve the homogeneity. The quality of the sample was verified through powder X-ray diffraction using a Panalytical X-Pert Pro diffractometer. The x-ray powder diffraction

(XRD) pattern of CeIr₂ is shown in Fig.1 (top) along with the simulated XRD pattern (bottom) using the cubic phase (space group $Fd\bar{3}m$, No. 227, with cubic lattice parameter $a=5.394$ Å). A very good agreement between the experimental XRD pattern and the simulated pattern indicates the single phase nature of CeIr₂ sample.

The heat capacity of CeIr₂ down to 400 mK was measured using a Quantum Design Physical Property Measurement System with a ³He insert. Fig.2 shows the temperature dependence heat capacity of CeIr₂ between 2.5 K and 400 mK in zero applied field. It is clear that the heat capacity decreases with decreasing temperature down to 400 mK. No clear sign of an onset of superconductivity was observed in the heat capacity of CeIr₂ down to 400m K, which suggests that superconducting transition temperature of our CeIr₂ sample is below 400 mK.

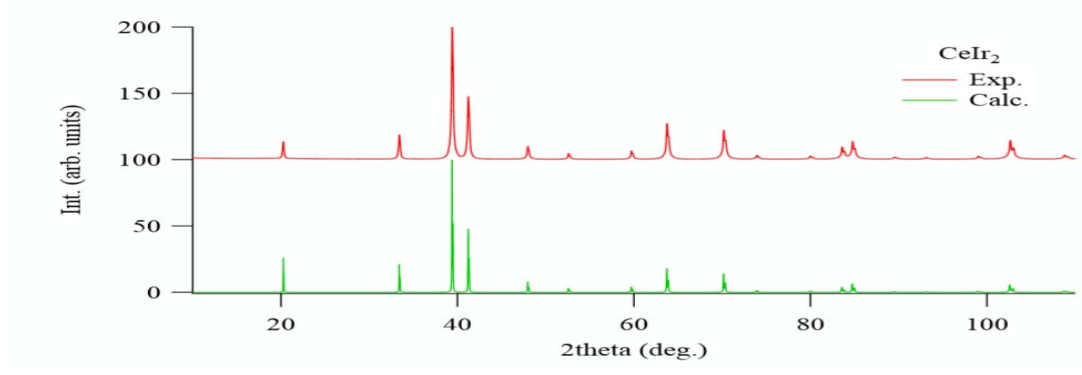


FIG. 5. (Color online)(top) The experimental X-ray diffraction pattern of CeIr_2 and (bottom) the simulated X-ray diffraction pattern of CeIr_2 using cubic phase (space group $Fd\bar{3}m$, No. 227).

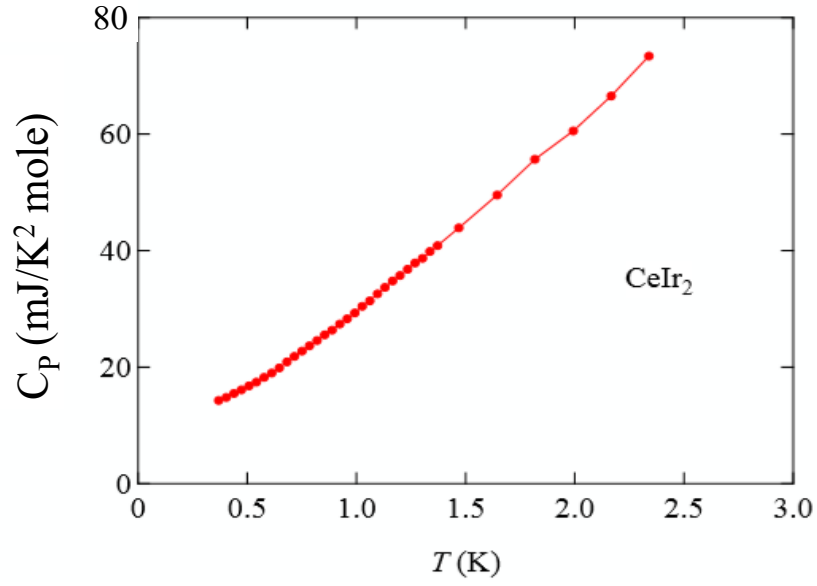


FIG. 6. (Color online)Temperature dependence of the heat capacity of CeIr_2 in zero applied field.